Fibers and Polymers 2018, Vol.19, No.10, 2066-2079
DOI 10.1007/s12221-018-8379-5

ISSN 1229-9197 (print version)
ISSN 1875-0052 (electronic version)

Incorporation of Functionalized Silica Nanoparticles into Polymeric Films for Enhancement of Water Absorption and Water Vapor Transition

Seyed Jalil Poormohammadian[1], Parviz Darvishi[1]*, Abdol Mohammad Ghalambor Dezfuli[2], and Mohammad Bonyadi[1]

[1]*Chemical Engineering Department, School of Engineering, Yasouj University, Yasouj 7591874934, Iran*
[2]*Physics Department, Faculty of Science, Shahid Chamran University of Ahvaz, Ahvaz 6135743135, Iran*

(Received May 9, 2018; Revised August 1, 2018; Accepted August 20, 2018)

Abstract: Water absorption and water vapor transition are significant mechanisms in many industrial processes. Nanocomposite polymers are appropriate materials for water transition process due to their specific properties. The present work was aimed to enhance the water absorption and water vapor transition by high loading incorporation of silica nanoparticles (NPs) into polyacrylonitrile (PAN) and Pebax 1657 polymers. PAN was used to prepare both the nanocomposite films (NCFs) and support layers of nanocomposite membranes (NCMs). Pebax 1657 was used to fabricate the selective layers of NCMs. Incorporation of NPs into the NCFs were carried out using ex-situ and in-situ (sol-gel) methods. NCFs were fabricated by electrospinning and casting methods. The fabricated NCFs of fibers and polymers were examined through water absorption tests. For fabrication of NCMs, the electrospinning and dip-coating methodologies and the incorporation of NPs into the selective layers by in-situ method were used. Besides, the water vapor permeation tests have been designed and constructed to examine the NCMs for dehydration of methane gas. In order to provide efficient NPs dispersion into NCFs, the surface functionalization of silica NPs with ethylene glycol (EG) was also considered. The functionalized silica NPs were used in the fabrication of NCFs and into the selective layer of NCMs. It is found that in applying the ex-situ method, there is a lot of NPs agglomeration, while the dispersion quality of NPs is higher with the sol-gel method. In addition, the dispersion is improved greatly with functionalization of silica NPs. The water uptake ratio of electrospun mats is about 400 % higher than the cast layers for the same loadings of NPs. The water uptake ratio of the polymeric layers containing EG is about 50 % higher than the samples without EG. The permeance of water vapor for the NCM (15 wt.% of SiO_2/Pebax 1657) fabricated by sol-gel method was enhanced to 54.4 % higher than the membranes without NPs. Functionalization of silica NPs also enhanced the water vapor permeation process. For instance, the water vapor of the NCM containing 30 wt.% of EG/Pebax1657 was increased by 68.7 %.

Keywords: Water transport, Nanoparticles dispersion, Fibers and polymeric films, Sol-gel method

Introduction

In the last two decades, practical use of inorganic nanoparticles has been increased in many fields such as adsorption, water treatment, membrane gas separation, medical and electronic devices. This great attention to these inorganic materials is due to their unique size-dependent properties mainly consist of chemical and optical properties [1,2], mechanical strength [3,4], electrical conductivity and high thermal stability [5,6]. Addition of metallic NPs to polymers can enhance their properties remarkably because of the high surface area to volume ratio of NPs [7,8]. On the other hand, polymeric nanocomposites are able to combine the advantages of excellent flexibility and ductility [4] with functional properties of NPs. This combination of properties can enhance the performance of many industrial processes such as gas dehydration, water absorption, and textile materials. Industrial textile processes require relatively large amounts of water, in which mass transport is often the rate-limiting step [9]. In order to achieve high water transition rates by the aid of NPs and polymeric materials, the dispersion quality of NPs into the polymer matrix should be improved. There are other applications that their functionality demands high inorganic material content [10,11] and carbon capture materials [12]. High loading of NPs into the polymers is limited due to the high tendency of NPs agglomeration. Therefore, to incorporate a high loading of NPs, the distribution uniformity and dispersion stability of NPs in the polymer matrix should be enhanced. For this reason, the selection of NPs materials, the method of NPs incorporation into the polymers and surface modification of NPs are the important factors that can help enhancing the NPs dispersion and water transition processes in and through the polymers.

The stable incorporation of appropriate NPs into the polymer has enhanced the properties of polymers in many fields. Sreekumar *et al.* [13] added single-walled carbon nanotube (SWNT) to PAN (10 wt.%) and in comparison to pure PAN a significant increase in tensile modulus, reduction in thermal shrinkage and glass transition temperature was achieved. Ge *et al.* [14] have shown that functionalization of PAN-based nanofiber with 20 wt.% multi-walled carbon nanotubes (MWNT) will enhance the electrical conductivity, mechanical properties, thermal deformation temperature, thermal stability and dimensional stability of the PAN polymer. In two other works, silver with an equal molar ratio

*Corresponding author: pdarvishi@yu.ac.ir

of acrylonitrile to silver nitrate [15] and titanium dioxide (6 wt.% in the PAN solution) [16] nanoparticles embedded in the PAN polymer and fine dispersion of nanoparticles was achieved. Bai *et al.* [17] dispersed AgCl with a different molar ratio (5, 10 and 20 %) to PAN polymer and suggested this nanocomposite polymer for the fields such as photonic, catalysts and electronics. Bonino *et al.* [18] incorporated tin oxide nanoparticles (1.9 to 8.6 wt.%) into PAN solution and showed the performance improvement of lithium ion battery anodes by increasing the conductivity from 0.03 (for pure PAN solution) to 0.11 mS cm^{-1} (for composite solution). Silica nanoparticles are also added to PAN polymer by some researchers [19-23]. Ji *et al.* [23] measured the surface area of the composite materials using the Brunauer-Emmett-Teller (BET) nitrogen adsorption method. They reported that the composite silica/PAN (5 wt.%) nanofibers have 20 % higher surface area in comparison to pure PAN nanofibers.

In order to reach high water transition rates in the membrane systems, the performance of both support and selective layers of the polymeric membranes should be improved. For this purpose, the thermodynamic interaction parameter between the selected materials should be enough to encounter specific interactions between the components and prepare the desired nanocomposite polymers for the process [24]. Van der Waals, electrostatic and hydration interactions between the polymers, NPs and water molecules are also important and should be considered in the selection of polymers and NPs [25,26]. Most of the previously fabricated polymeric membranes for water vapor transition had a microporous support layer, which acts as a barrier for H_2O molecules. Since these support layers are made by casting of polymer solutions, they usually have a low porosity. In addition, the high condensability of water molecules limits their transportation through the layers because of the well-known concentration polarization phenomena [27]. At the best-operating conditions, about 30 % of the water vapor transmission resistance is contributed by selective layers and 70 % is of support layers [27,28]. An efficient method that may help to overcome this problem is the application of nanostructured polymers (NSPs) as construction materials. Among various techniques have been considered for preparing NSPs, nanoscale polymers and nanofibers are widely investigated and applied [29]. Previous studies have shown that polymeric nanofibers (PNFs) will have a set of favorable properties such as high porosity, outstanding mechanical and thermodynamic properties, and increased surface-to-volume ratio [29]. A number of methods are used for the synthesis of PNFs, among them electrospinning process seems to be the only approach that can be used for massive production. Based on the obtained results in our previous work [30], the electrospun PAN showed a satisfactory performance in the water vapor transmission process due to its very low Flory-Huggins interaction parameter with water molecules that makes it to be a good candidate for the mechanisms relevant to water operations. It is a superabsorbent semi-crystalline polymer [31,32] that consists of high polar nitrile groups and dipole moment, and it can be a reasonable choice for fabricating high porous support layers via electrospinning methodology.

Polymeric membrane selective layers play the basic role in the gas separation process. The efficiency of the water vapor separation in the membrane selective layers may be improved by selecting a suitable material and finding a reliable technique for incorporating the NPs into the polymer matrix. Among the hydrophilic rubbery polymers, Pebax 1657 is a qualified and suitable polymer for manufacturing the membrane selective layer. It has been attracted significant interest for water vapor transition and specially dehydration of permanent gases such as nitrogen and methane [33-35]. It consists of a hydrophilic polyethylene oxide (PEO) phase and a rigid glassy polyamide phase. The hydrophilic rubbery PEO phase provides good separation properties for H_2O/CH_4, and the rigid glassy phase provides good mechanical properties for operation at high pressures and high water contents [36].

Selection of the NPs is also very essential for water transition treatment. Each nanofiller has its specific application in the industry based on its properties. Most of nanomaterials can increase the surface porosity of polymers and improve their properties [37]. Beside, nanofillers can steer the spatial distribution of polymeric chains and increase their free volume [38]. Metal-organic frameworks (MOFs) are made by linking inorganic and organic units through strong bonds. The high surface area, tunable porosity, and diversity in metal and functional groups make them attractive to use as catalysts but their applications are not commercialized [39]. They are good adsorbents in water-based adsorption heat pumps in comparison to traditional zeolites and activated carbon materials [40,41]. MOFs can also be used for gas storage, purification and separation, and sensing applications but they are crystalline materials [42] and incorporation of them into the polymer matrix will enhance the crystallinity of the polymers. Carbon nanotubes (CNTs) have high transport diffusivities of light gases in comparison to zeolites of similar pore sizes [43]. In addition, CNTs have a double adsorption capacity compared to activated carbons [44], but they are expensive sorbents [45]. Due to the nature of water molecules, the hydrophilicity and polar surface energy of incorporated NPs are the dominant factors in the water absorption process. Silica NPs are highly hydrophilic materials in comparison to activated carbon [46] and the specific or polar component of the surface energy, which is estimated from the specific interaction between the filler surface and polar chemicals, is much higher for silica than carbon black [47]. Therefore, silica NPs can interact very well with polymers such as PAN that have highly polar groups in their structure. This leads to a strong hydrogen bonding between the polymer nitrile groups and -Si-OH group on the silica

surface. On the other hand, silica NPs have unique properties that make them specific for water absorption and water vapor transmission applications. These properties include high surface area, inert nature, low toxicity, thermal stability, facile synthetic route, large-scale synthetic ability and the ability to be functionalized with a wide range of polymer molecules [21-23,48]. These properties allow the nano-composite polymers to have improved properties of hydrophilicity, toughness, and permeability [49-52].

Methods of NPs incorporation can affect the dispersion of NPs significantly. Generally, there are two completely different methods for incorporation of NPs into the polymer matrix. In the first method which is called ex-situ method, the inorganic NPs and polymer solution are blended after they are synthesized individually [53]. In the solution, the NPs are in the form of colloid, and the incorporation process depends on the surface tension of polymer solution as well as the wettability between the solid particles and the solution [54]. Although some nanoparticles have good compatibility with specific polymer solutions, a non-uniformity may achieve in small amounts of NPs which leads to the agglomeration of inorganic materials in the matrix [23]. In the second method which is called in-situ method, NPs are synthesized inside the polymer matrix through the sol-gel process [55,56]. A precursor is used as the nanoparticle source, and during the hydrolysis and condensation reaction, the NPs are synthesized in the proper solvent. Since the metallic precursor must be soluble in the solvent, the selection of solvent is important. The method is simple, convenient and leads to the production of inorganic materials with uniform size and shape [57]. The sol-gel matrix can disturb the reticulation and agglomeration process of the NPs [58], where the fabrication of NPs is inside the polymer solution. Therefore, optimal bonding between the polymer matrix and inorganic NPs as well as the improvement of NPs dispersion can be expected.

Functionalization of NPs, which allows modifying and controlling their properties is another effective methodology to enhance the dispersion of NPs. This process is carried out by surface coating of NPs with another chemical group which assists to regulate the properties of NPs for target characteristics. Selection of the chemicals for surface modification of NPs is also important. Chemical surfactants have been used for efficient dispersion of NPs by some researchers [59,60] but these chemicals can lead to harmful environmental impacts [61].

This work is aimed to improve the water absorption and water vapor transition into and through the polymers. For this purpose, three techniques of electrospinning methodology, high incorporation of silica NPs into the polymer and functionalization of silica NPs by EG were applied. At first, the dispersion of silica NPs into the casted and electrospun polymeric films of PAN with ex-situ and in-situ methods was investigated. Then, the functionalization of silica NPs by EG was applied to achieve a reasonable quality of dispersion at high loadings of NPs into the NCFs. The required analysis including XRD, FESEM and FTIR of samples were taken to demonstrate the effect of examined methods on NPs dispersion and structure of polymers. The fabricated NCFs were tested through water absorption tests and compared with each other to show the effect of each technique on water absorption process. Having found the best strategy, NCMs of Pebax 1657 were fabricated, and silica NPs and functionalized silica NPs were incorporated into the selective layers of NCMs using in-situ method. The fabricated NCMs of Pebax 1657 copolymer were used for dehydration of methane gas in a water vapor permeation set-up.

Experimental

Chemicals

Polyacrylonitrile (PAN, average M_w=100000) was provided from Esfahan Polyacryl Company, Iran. Pebax 1657 was purchased from Arkema, France. Tetraethyl orthosilicate (TEOS) 95 % as silica precursor, ethanol (99.9 wt.%), and N, N-dimethylformamide (DMF) with purity of 99 wt.% were supplied from Samchun, Korea. Hydrochloric acid (HCl) 37 wt.% and EG (99.8 wt.%) were purchased from Merck, and silica NPs were provided from Tecnan, Spain. Nitrogen with a purity of 99.9 % and methane with a purity of 99.95 % were purchased from Farafan gas, Iran. All chemicals were used as received without further purification.

Nanocomposite Films Preparation

To show and compare the effect of the new methods for water absorption in comparison to the traditional ones, three important categories were investigated in the fabrication of NCFs, including electrospinning and/or casting method, in-situ (sol-gel) and ex-situ incorporation methods and functionalization of silica NPs by EG. For each category, the pertinent polymer solutions (including different amount of silica NPs) were prepared via the specific procedure and the NCFs were fabricated by casting and electrospinning methods. The detailed description of the NCFs preparation is described in the following order. All of the as-prepared NCFs were tested and compared for water absorption process.

PAN solution was prepared by mixing 10 wt.% of PAN powder with DMF, and stirred at 60 ^{o}C for 6 h until a well-dissolved solution with light yellow color was achieved. Stirring was continued at room temperature overnight. A casted (FM18) and electrospun (FM17) film of this solution without NPs were prepared to compare with each other and with the NCFs containing silica NPs. The silica NPs were incorporated into PAN solution to find the best way of NPs incorporation based on the following procedures.

In the first method, silica NPs were added to DMF and

stirred for 30 min. Then, the PAN solution was added to obtain 5 and 15 wt.% of SiO_2/PAN solutions. Finally, the solution was stirred vigorously for 12 h and ultra-sonicated for 60 min after each 3 h stirring. Nanocomposite films of the prepared solutions were fabricated by casting and electrospinning methods (FM1-FM4).

In the next method, the sol-gel was utilized to synthesize the silica nanoparticles based on Stöber method [62]. Different amounts of TEOS were dissolved in DMF and stirred at room temperature for 30 min. Then, HCl is added dropwise to reach a concentration of 0.1 M followed by stirring at 60 °C for 2 h. Finally, the PAN solution was gradually added and the mixture was thoroughly mixed for 60 min by stirring at 60 °C. The nanocomposite films (FM5-FM12) of this method were also fabricated by casting and electrospinning of the polymer solutions.

In the last technique, to functionalize the silica NPs, EG was added to the solutions prepared by the sol-gel method. After the addition of HCl, EG was added to the solutions and stirred for 2 h at 60 °C. Finally, the PAN solution was added and stirred for 60 min at 60 °C. Since the surface tension of EG is higher than the PAN solution, the addition of EG increases the surface tension of the solutions and these solutions cannot be electrospun even at high DC voltages. Therefore, only the casted films (FM13-FM-16) were fabricated for these polymer solutions. The details of chemicals used for preparation of all fabricated polymeric films (FM1-FM18) is summarized in Table 1.

For electrospinning of the polymer solutions, an electrospinning set-up was used, as described in our previous work [30]. The feed rate of the solution was kept constant at 0.5 m*l* h^{-1} for nanocomposite films and 1.2 m*l* h^{-1} for pure PAN solution (without NPs) using a controlled syringe pump. The distance from the spinneret to the collector was fixed at 15 cm. To prepare the casted NCFs, polymer solutions were casted using a blade at 200 μm above the glass plate. Then, the glass plates were immersed for 24 h in a deionized water bath to remove the solvent. Finally, the casted films were dried at room temperature for 24 h.

Films Characterization

Field emission electron microscopy (Hitachi S 4160 FESEM, Japan) was used to examine the surface morphology of PAN nanofibers and silica NPs incorporated into PAN polymeric films. X-ray diffractometer (Philips PW1830, Netherlands) was used to investigate the phase and crystalline state of the NCFs. The surface chemistry of nanofibers and NCFs was examined by Fourier transform infrared spectroscopy (ABB, BOMEM 102, Canada) in the range of 4000-400 cm^{-1}.

Water Uptake Measurement

The method of Kiatkamjornwong *et al.* [63] was used to measure the water absorption capacity of the NCFs. The

Table 1. Chemicals used for the preparation of nanocomposite films

	DMF (g)	TEOS (g)[a]	HCL (g) (37 wt.%)	Silica NPs (g)	EG (g)	PAN sol. (g)	Fabrication method
FM1	10	-	-	0.05	-	10	Cas.[b]
FM2	10	-	-	0.05	-	10	Elec.[c]
FM3	10	-	-	0.15	-	10	Cas.
FM4	10	-	-	0.15	-	10	Elec.
FM5	10	0.178	0.107	-	-	10	Cas.
FM6	10	0.178	0.107	-	-	10	Elec.
FM7	10	0.535	0.111	-	-	10	Cas.
FM8	10	0.535	0.111	-	-	10	Elec.
FM9	10	1.07	0.117	-	-	10	Cas.
FM10	10	1.07	0.117	-	-	10	Elec.
FM11	10	1.785	0.125	-	-	10	Cas.
FM12	10	1.785	0.125	-	-	10	Elec.
FM13	10	1.785	0.129	-	0.5	10	Cas.
FM14	10	1.785	0.133	-	1.0	10	Cas.
FM15	10	1.785	0.138	-	1.5	10	Cas.
FM16	10	1.785	0.142	-	2.0	10	Cas.
FM17	-	-	-	-	-	10	Elec.
FM18	-	-	-	-	-	10	Cas.

[a]Each gram of TEOS contains 0.28 gram SiO_2, [b]casting, and [c]electrospinning.

specimens of each film were cut (40 mm×50 mm) and dried for 24 h above the glass transition temperature of PAN to obtain the initial mass (W_1) of each sample. Then, the dried film was immersed in deionized water for 24 h under controlled temperature conditions. After that, the samples were weighed (W_2) to obtain the soaked weight of swollen films. The water uptake ratio was calculated from equation (1):

$$\Delta w = \frac{w_2 - w_1}{w_1} \times 100 \quad (1)$$

And, the porosity was calculated using the following equation [64]:

$$ø\ (\%) = \left(\frac{w_2 - w_1}{\mathrm{Al}\rho}\right) \times 100 \quad (2)$$

Each test of water uptake measurement was carried out four times to decrease the uncertainty of experiments. Each measured data point in the current study is the average of at least four independent measurements. Besides, along with each data points, error bars are indicated for better comparison between the different cases.

Nanocomposite Membrane Preparation

As discussed earlier, the composite and nanocomposite polymeric membranes usually consist of two main layers. Due to much better performance of electrospun support layers in water vapor transition compared to casted supports [30], the support layers were prepared by electrospinning methodology. In order to gain more mechanical strength of the membranes, PAN solutions were electrospun on a porous polyester layer.

Before fabricating the selective layers of the NCMs, we investigated the results of the NPs distribution into the NCFs and the water uptake measurements of the NCFs. Based on the obtained results from the previous sections, we utilized the in-situ method (sol-gel and functionalized silica NPs) to incorporate silica NPs into the membrane selective layer solutions. To this end, Pebax 1657 solutions for fabrication of selective layers were prepared by mixing 2 wt.% of Pebax granules in a solvent mixture of deionized water and ethanol (70 vol.% of ethanol) and stirred for 12 h at 90 °C. Then, different amounts of TEOS, HCL and EG were added to Pebax 1657 solution via in-situ method and deposited on the fabricated electrospun support layers of PAN using dip-coating process. The detailed properties of nanocomposite selective layers are presented in Table 2.

Water Vapor Permeation Tests

The fabricated NCMs were tested using a typical gas permeation set-up (Figure 1) for measuring the permeability of water vapor. Pure methane gas was introduced into a water bubbler at a controlled temperature to produce the wet gas. Then, the wet gas stream was entered a demister to capture any liquid mist. The permeation cell was modified under sweep/countercurrent conditions to enhance the

Table 2. Properties of nanocomposite membrane selective layers

	Mem 1	Mem 2	Mem 3	Mem 4	Mem 5	Mem 6
Incorporation method	No nanoparticle	Sol-gel	Sol-gel	Sol-gel	Func. SiO_2	Func. SiO_2
SiO_2/Pebax (wt.%)	-	5	15	30	30	30
EG/Pebax (wt.%)	-	-	-	-	10	30

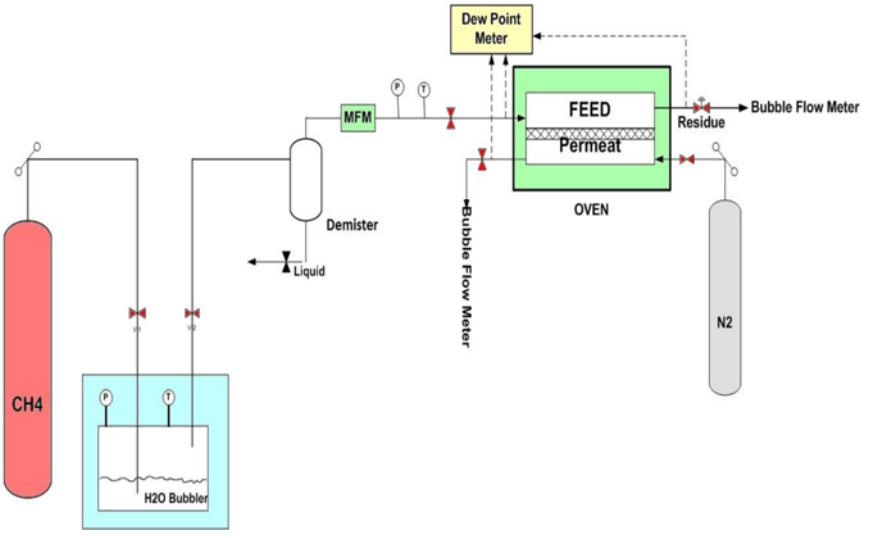

Figure 1. Water vapor permeation set-up.

permeation of water vapor through the nanocomposite membranes. The water content in the feed, retentate and permeate streams was measured using a dew point sensor (S212, CSi-tec, Germany, measurement range: 0-100 RH%). The feed flow rate was measured with a mass flow meter (S420, CSi-tec, Germany, measurement range: 0-60 NL min^{-1}). The membrane permeation cell was fabricated from stainless steel and all sides of the membrane were sealed by o-rings. The membrane sheet with an active area of 157 cm^2 was supported by a rectangular porous plate made from stainless steel to withstand the feed side pressure mounted in the cell.

The permeability of a polymeric film to gas molecules is determined by the following equation:

$$P = \frac{Nl}{A(p_2 - p_1)} \quad (3)$$

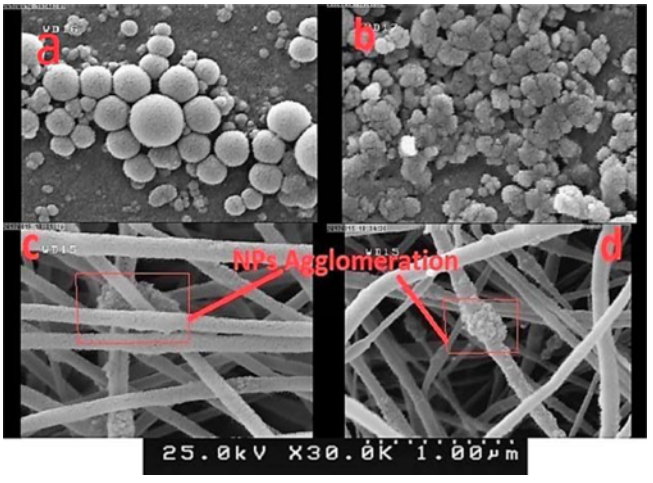

Figure 2. FESEM images of the nanocomposite films; (a) FM1, (b) FM3, (c) FM2, and (d) FM4. The zone magnification is 30000 and the scale bar is 1 μm.

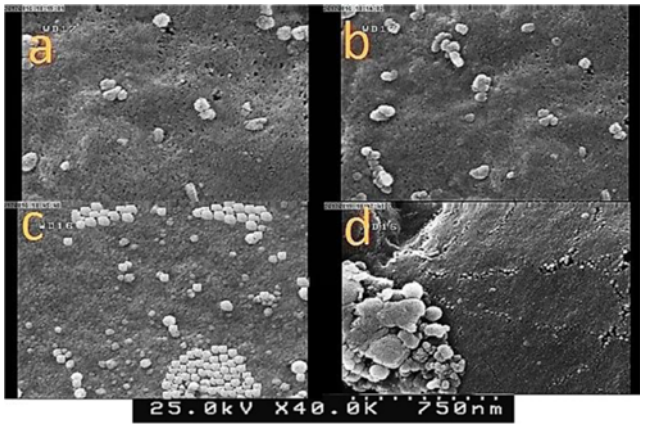

Figure 3. FESEM of the casted nanocomposite films; (a) FM5, (b) FM7, (c) FM9, and (d) FM11. The zone magnification is 40000 and the scale bar is 750 nm.

Permeability coefficient is usually expressed in units of barrers, where 1 barrer=$10^{-10}$$cm^3$ (STP) $cm^{-2}s^{-1}$ (cm Hg)$^{-1}$. For comparison of thin films with different thicknesses, permeance is used instead of permeability, which is defined as permeability over the film thickness (P/l) and is often expressed in gas permeation units (gpu), where 1 gpu= $10^{-6}$$cm^3$ (STP) $cm^{-2}s^{-1}$ (cm Hg)$^{-1}$.

Results and Discussion

Films Characterization

Figure 2 shows the FESEM images of four nanocomposite films (FM1-FM4) fabricated by adding silica NPs to PAN solutions. As it is shown, the ex-situ incorporation method of NPs into polymeric solutions is not appropriate due to high agglomeration of NPs. The agglomeration of silica NPs is much higher in Figure 2(b) (15 wt.% of SiO_2/PAN) than Figure 2(a) (5 wt.% of SiO_2/PAN). Figure 2(c) and (d) represent the same loadings of silica NPs as Figure 2(a) and (b), respectively but these layers were fabricated using the electrospinning method. Although the aggregation of silica NPs is lower than casted films, the NPs agglomeration is still observed in some areas.

Figure 3(a) and (b) demonstrate the FESEM images of casted nanocomposite films fabricated by the sol-gel method. The dispersion of NPs is appropriate in 5 and 15 wt.% concentrations of SiO_2 in the PAN polymer. As it is shown in Figure 3(c), at higher loading of NPs (30 wt.% of SiO_2/PAN), the agglomeration is increased and in 50 wt.% of the SiO_2/PAN composition (Figure 3(d)), the dispersion of NPs is failed and high agglomerations of NPs are achieved. Therefore, the sol-gel (in-situ) method improves the dispersion of NPs with respect to conventional ex-situ ones, but at higher loadings of NPs (more than 30 wt.% of SiO_2/PAN composition), another effective technique should be considered.

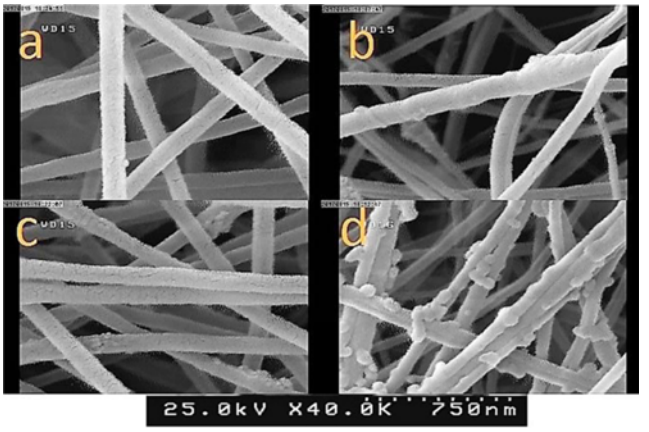

Figure 4. FESEM of the electrospun nanocomposite films; (a) FM6, (b) FM8, (c) FM10, and (d) FM12. The zone magnification is 40000 and the scale bar is 750 nm.

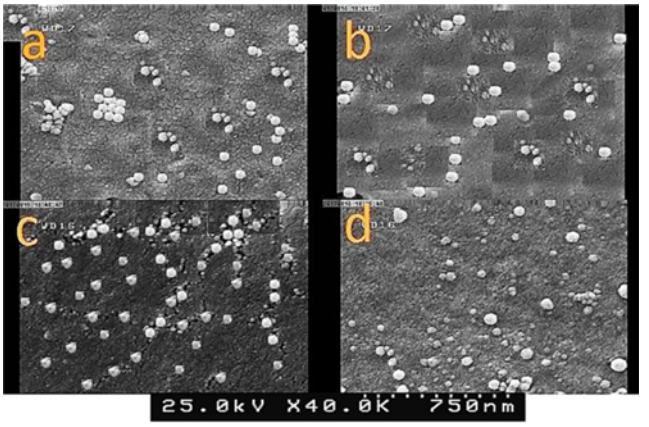

Figure 5. FESEM of the casted nanocomposite films; (a) FM13, (b) FM14, (c) FM15, and (d) FM16. The zone magnification is 40000 and the scale bar is 750 nm.

Figure 4 indicates the effect of electrospinning methodology on the dispersion of NPs in the polymeric films fabricated by the sol-gel method. It is clear that up to 30 wt.% of SiO_2/PAN composition, there is no significant agglomeration of NPs. In 50 wt.% of SiO_2/PAN loading (Figure 4(d)), the adhesion of NPs is observed, but it is distributed among all nanofibers. The synthesized silica NPs became a part of the polymer chain and the electrospinning methodology causes the NPs to be blocked within the polymeric nanofibers. In comparison of Figures (3) and (4), it is concluded that for the same loading of NPs, the electrospun nanocomposite layers include much better NPs dispersion with respect to casted layers.

The effect of functionalization of silica NPs has been examined by addition of EG to the solutions prepared by sol-gel method. The FESEM images of the casted nanocomposite films are shown in Figure 5. In all of the four prepared solutions, the amount of silica NPs loading is high (50 wt.% of the SiO_2/PAN composition) and the amount of EG is increased from 25 to 100 wt.% of EG/silica. The pictures reveal that addition of EG improves the dispersion of silica NPs with respect to solutions do not contain EG (Figure 3(d)). There is a little NPs agglomeration in Figure 5(a) (25 wt.% of EG/silica), but it is eliminated when using higher amounts of EG.

After calibration of the images based on their scale bars, the nanofiber diameter of electrospun mats was measured using KLONK image software. For each of electrospun NCFs, the average diameter of 100 different nanofibers was determined. The thickness of NCFs needed for porosity calculations was measured using a micrometer (Mitutoyo MDC 0-1 PF, Japan) at ten different locations and the average value was calculated. The average diameter, thickness, and porosity of NCFs with their standard deviations are reported in Table 3.

A comparison between Figure 3(a) and 4(a) or Figure 3(b) and 4(b) with the same amounts of silica NPs shows that electrospun films are highly porous with respect to casted layers. It is due to the polymer nanoscale size and inherent characteristics of the electrospinning methodology. To check the effect of doping silica NPs on the properties of casted layers, the cross sectional images of some samples are taken and shown in Figure 6. The cross sections are pertinent to FM18 (the cast without NPs), FM5, FM7 and FM9. As it seen, increasing the concentration of silica NPs in the matrix

Table 3. The characteristics of nanocomposite films

	Fiber diameter (nm)	Thickness (μm)	Porosity (%)
FM1	-	82±6	48.8±2.6
FM2	255±25	76±4	86.3±3.3
FM3	-	81±5	53.6±2.8
FM4	260±40	84±5	89.4±3.7
FM5	-	96±4	52.3±2.5
FM6	290±35	83±4	88.3±4.3
FM7	-	87±3	58.2±3.0
FM8	315±50	72±3	91.3±4.6
FM9	-	85±4	62.1±3.4
FM10	345±60	77±3	93.5±5.2
FM11	-	90±5	68.6±3.5
FM12	340±70	82±4	94.6±4.8
FM13	-	88±5	71.2±3.7
FM14	-	94±6	72.3±3.5
FM15	-	102±7	74.2±3.9
FM16	-	83±5	73.7±4.1
FM17	250±30	79±4	78.4±4.4
FM18	-	86±5	42.7±2.3

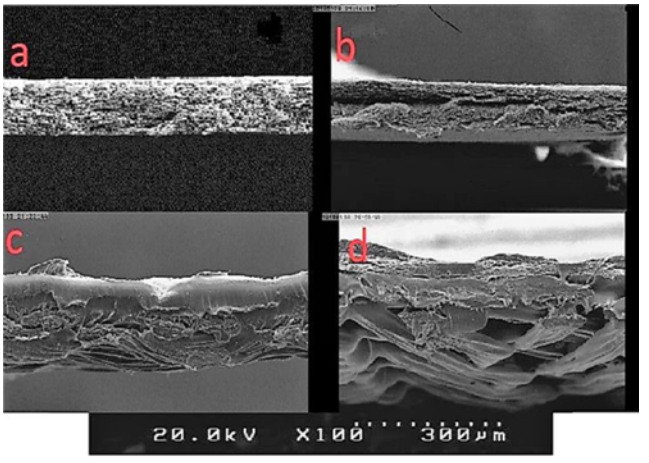

Figure 6. Cross section images of (a) FM18, (b) FM5, (c) FM7, and (d) FM9. It is seen that the pores become larger by increase in the silica NPs.

Table 4. Fractional free volume of the nanocomposite films

	FM18	FM1	FM3	FM9	FM11	FM13	FM14	FM15	FM16
FFV	0.057	0.079	0.106	0.143	0.189	0.204	0.221	0.245	0.271
	MEM1	MEM2	MEM3	MEM4	MEM5	MEM6			
FFV	0.102	0.143	0.171	0.202	0.226	0.247			

of polymer contributes to more and larger pores in the structure of polymer, leading to an increase in the porosity of the films.

Another characteristic that shows the effect of doping silica NPs on the porosity of samples is the fractional free volume (FFV) of polymer, which is an intrinsic property created by the volume left between the entangled chains of polymer. The simplest and most used way to calculate this property for pure polymer without NPs is as follows [65]:

$$FFV = \frac{M_p/\rho_p - 1.3\,V_{w,p}}{M_p/\rho_p} \quad (4)$$

where M_p is the molar weight of polymer monomer (g mol^{-1}), ρ_p is the density of pure polymer (g cm^{-3}), and $V_{w,p}$ is the van der Waals volume of the polymer (cm^{3}mol^{-1}). The value of V_W=32.5 cm^{3}mol^{-1} is obtained for PAN based on Bondi's group contribution method [66,67]. For fabricated NCFs, the contribution of silica NPs should be taken into account, which can be calculated from the following equation [68]:

$$FFV = \frac{V_{NCFs} - \left[\left(\frac{1.3\,V_{w,p}}{M_p}\right)(1-\varphi_{sio2}) + \left(\frac{\varphi_{sio2}}{\rho_{sio2}}\right)\right]}{V_{NCFs}} \quad (5)$$

where V_{NCFs} is the specific volume of NCFs (cm^{3}g^{-1}) and φ_{sio2} is the volume fraction of silica NPs in the sample. The calculated FFVs for pure PAN and NCFs are presented in Table 4. As can be seen, there is an increasing trend for the calculated FFVs by increasing the concentration of silica NPs. This increase in FFVs of NCFs can be a proof for the improvement of their properties with respect to polymers without NPs (FM18). Based on the amount of silica NPs in the samples, the FFV of FM17, FM2/FM5/FM6, FM7/FM8, FM10, and FM12 are the same as the FFV of FM18, FM1, FM3, FM9, and FM11, respectively.

XRD Patterns

Figure 7 illustrates the XRD pattern of pure PAN, the SiO_2/PAN nanocomposite films with different loadings of silica NPs and the sample containing EG. The XRD pattern of pure casted PAN exhibits a peak at 2θ=17°. The sharp peak of 17° corresponds to plane (0 1 0) with a d-spacing of 5.30 °C that verifies the crystalline behavior of PAN [22,69]. Therefore, the pure casted PAN film (FM18) still keeps the crystalline structure. As it is observed, the peak at 2θ=17° becomes weak by addition of inorganic silica NPs and this attenuation is more revealed at higher loadings of silica NPs. There is also a weak and broad peak at 2θ=28° in the

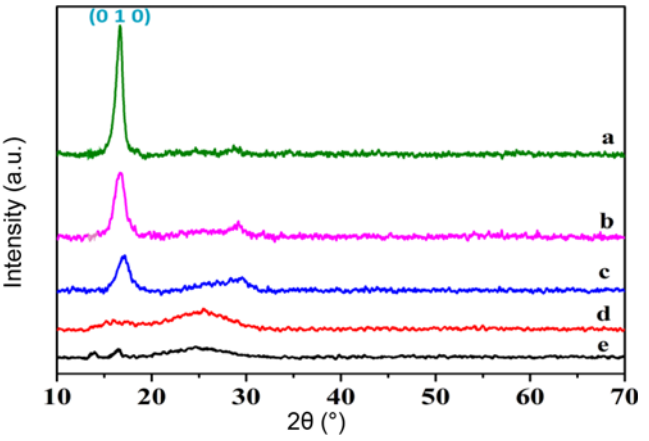

Figure 7. XRD patterns of nanocomposite films (a) pure PAN (FM18), (b) FM5 (5 wt.% SiO_2), (c) FM7 (15 wt.% SiO_2), (d) FM9 (50 wt.% SiO_2), and (e) FM14 (50 wt.% SiO_2 with equal amount of EG).

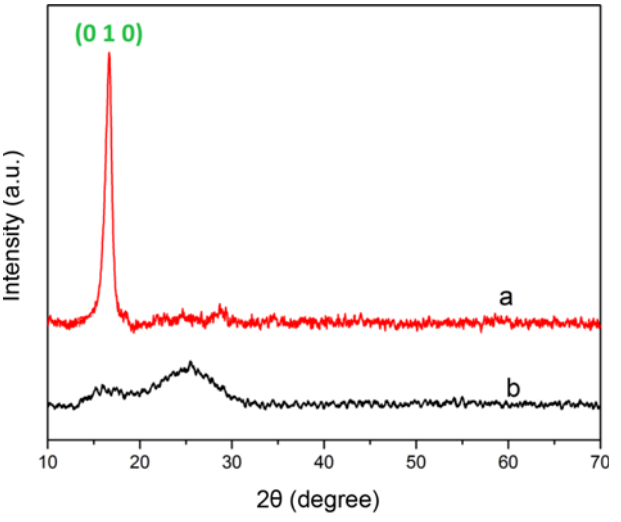

Figure 8. XRD pattern of polymeric films; (a) casted PAN (FM18) and (b) electrospun PAN (FM17).

samples containing silica NPs. This indicates that addition of inorganic fillers enhances the amorphous region in the PAN films. Addition of EG to nanocomposite polymeric films also decreases more the crystalline evidence of the peak at 2θ=17°, implying that better dispersion of hydrophilic fumed silica to composite solutions enhances the amorphous phase in the composite films [22].

To show the effect of electrospinning method with respect

to casted one, the XRD pattern of pure electrospun is compared with casted PAN films in Figure 8. It indicates that electrospun PAN has an amorphous structure, while the casted film exhibits crystalline structure [70]. The induced crystallinity of casted films reduces the free energy of mixing and hence the water uptake [71].

FTIR Spectra

The surface chemistry of nanocomposite films is examined by FTIR in the range 4000 to 400 cm^{-1}. Figure 9 illustrates the FTIR of FM1-FM4 films and the pure PAN. As shown in Figure 9(a), the band at 2940 cm^{-1} is related to -CH_2 group, while that at 2244 cm^{-1} is ascribed to nitrile groups. The absorption band at about 1735 cm^{-1} is attributed to C=O stretching vibration [69] and 1600 cm^{-1} is related to the C=C band, 1452-1500 cm^{-1} is ascribed to C-C stretching vibrations and 1255-1387 cm^{-1} is assigned to C-H bending vibrations. All of these bands reveal the chemical structure of PAN nanofibers [72,73]. Figure 9(b), (c), (d) and (e) are pertinent to FM1, FM2, FM3 and, FM4, respectively. Consequently, the addition of silica NPs to PAN solutions does not change the surface chemistry of PAN nanocomposite films and there are no new bands in the films. Thus, incorporation of silica NPs to PAN polymer via ex-situ method only cause the silica NPs to absorb physically and there is no evidence of chemical bands in this incorporation method.

Figure 10 shows the FTIR of nanocomposite films fabricated by the sol-gel method. The FTIR of casted and electrospun nanocomposite films are the same for an equivalent concentration of NPs. In addition to the bands of pure PAN (Figure 10(a)), some new bands are presented. The band at 3411 cm^{-1} in Figure 10(b) to (e) is ascribed to O-H group which is presented during hydrolysis step of the sol-gel method. The asymmetric and symmetric stretching of

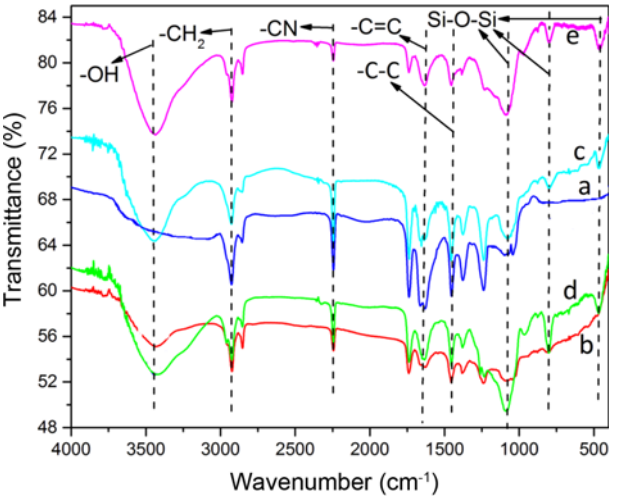

Figure 10. FTIR spectra of nanocomposite films of (a) pure PAN, (b) FM5 and FM6, (c) FM7 and FM8, (d) FM9 and FM10, and (e) FM11 and FM12.

Si-O-Si are presented at 1100 cm^{-1} and 800 cm^{-1}, respectively. The Si-O-Si bending is observed at 470 cm^{-1}, suggesting that SiO_2 is successfully grafted into the polymer matrix. The peaks of SiO_2 are gradually strengthened by increasing the SiO_2 load.

Figure 11 indicates the FTIR of functionalized silica NPs into the PAN polymers by EG. It is clear that all the bands of the sol-gel method can be observed in the figure. In addition to the bands of Figure 10, there is a new band around the 1000 cm^{-1} wave number that is assigned to functionalization of silica NPs. The peak of silica NPs functionalization is related to Si-O-CH_2 group which is strengthened by higher concentrations of EG.

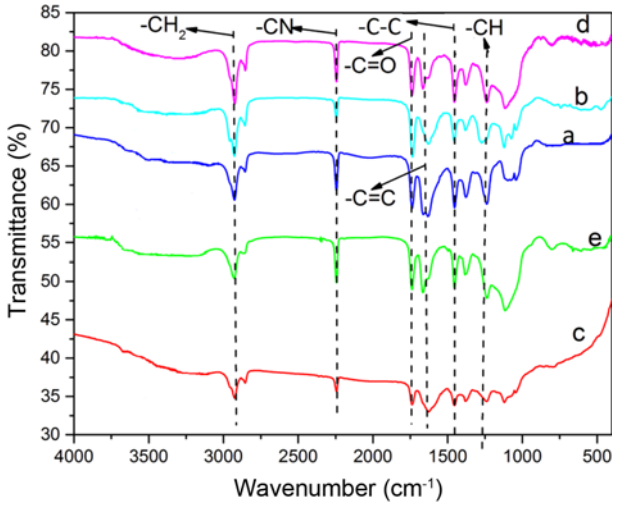

Figure 9. FTIR spectra of nanocomposite films of (a) pure PAN (FM17 and 18), (b) FM1, (c) FM3, (d) FM2, and (e) FM4.

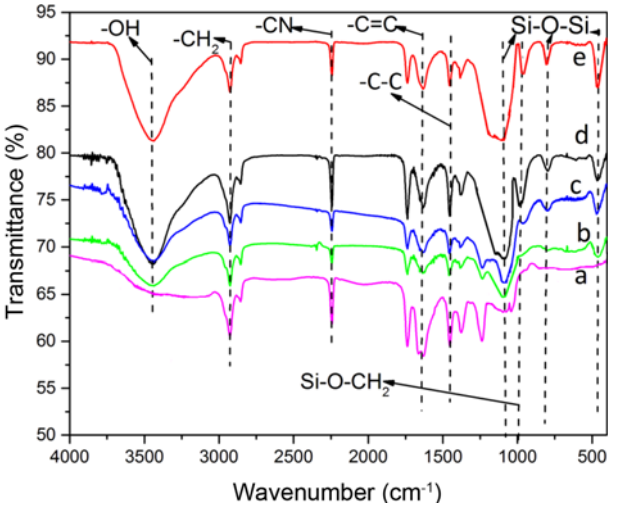

Figure 11. FTIR spectra of nanocomposite films of (a) pure PAN, (b) FM13, (c) FM14, (d) FM15, and (e) FM16.

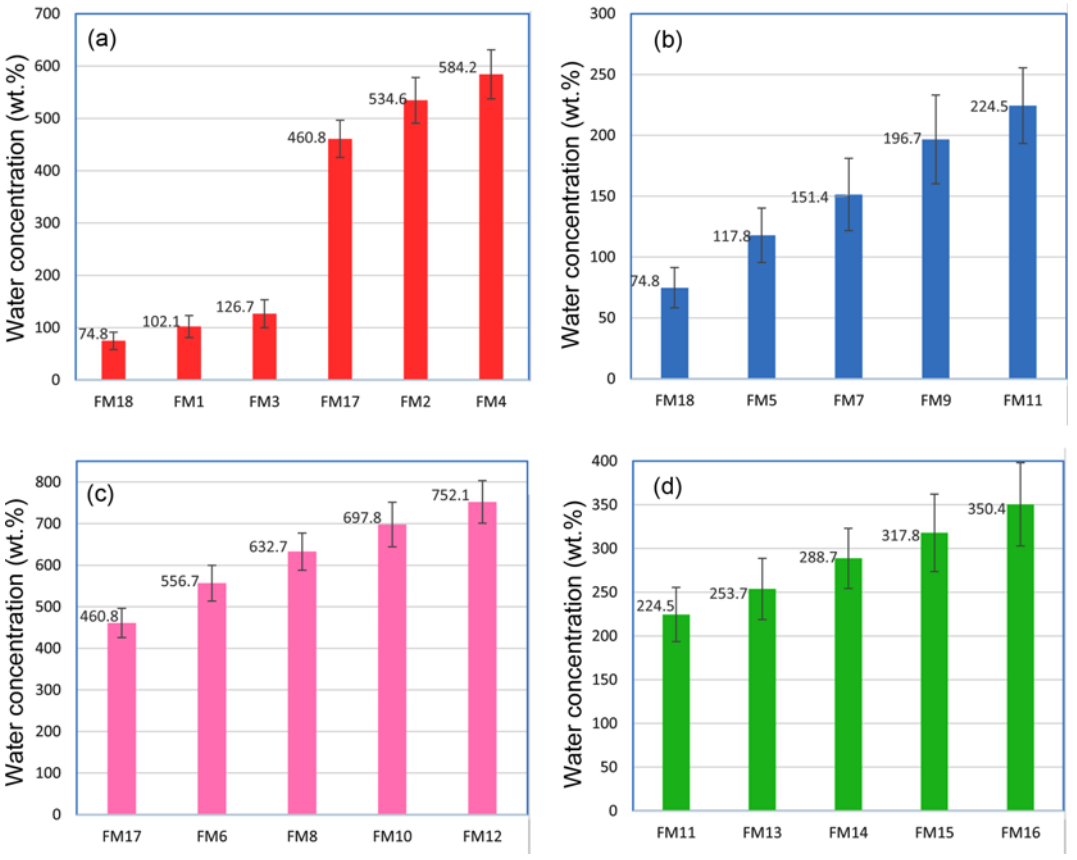

Figure 12. Water uptake ratio of nanocomposite films; (a) FM18, FM1, FM3, FM17, FM2 and FM4, (b) FM18, FM5, FM17, FM9, and FM11, (c) FM17, FM6, FM8, FM10, and FM12, and (d) FM13-FM16.

The Water Uptake Ratio of Nanocomposite Films

The capacity of fabricated NCFs for water absorption is shown in Figure 12 as water uptake ratio. The figure is divided into four parts to show the effect of each technique used in this study individually and clearly. The effect of electrospinning, incorporating of silica NPs (both ex-situ and in-situ methods), and functionalization of silica NPs has been shown and discussed separately.

Effect of Electrospinning Methodology

To show the effect of electrospinning methodology, the casted (FM18) and the electrospun (FM17) polymeric films are compared with each other in Figure 12(a). It is seen that electrospun mat absorbs much higher water. The reason is the higher porosity and nanoscale size of electrospun films, causing the interaction surface of the polymer with water molecules to be much higher than the semi-porous casted ones. Electrospun nanofibers are able to create a specific surface area of 1000 m^2g^{-1} which result in much higher surfaces of the polymer that can be exposed to water molecules [29,74]. Another reason for this difference is the amorphous structure of electrospun nanofiber films in contrast to the crystalline behavior of the casted films [71].

Effect of Ex-situ Incorporation Method

The water uptake ratio for the casted film without NPs (FM18) is 74.8 %, which is indicated in Figure 12(a). Tripathi *et al.* [64] obtained a value of 93.1 % for PAN casted film. The difference can be due to the porosity of the fabricated films. The porosity of their film was 51.7 %, which was higher than the porosity (42.7 %) of the casted film prepared in the present research. In comparison of FM1 and FM3 to FM 18 in Figure 12(a), it can be seen that the concentration of water is increased about 36.5 percent for FM1 (5 wt.% of SiO_2/PAN) and 70 percent for FM3 (15 wt.% of SiO_2/PAN) with respect to FM18. Both of FM1 and FM3 as well as FM18 are fabricated by cast method and have the same structure. Similar results are obtained for the electrospun films of FM2 and FM4 in comparison to FM17. The water uptake ratio has been increased by 16 % for FM2 (5 wt.% of SiO_2/PAN) and by 26.7 % for FM4 (15 wt.% of SiO_2/PAN) in comparison to FM17. These three polymeric films also have the same structure. The reason of high water absorption is the hydrophilic nature, high surface area to volume ratio of silica NPs and the porosity of the films, which is increased by the addition of silica NPs to the

solutions.

Effect of In-situ Incorporation Method

The water uptake ratio of the casted and electrospun films fabricated by the sol-gel method is indicated in Figure 12(b) and (c), respectively. Both casted and electrospun films of the sol-gel method absorb more water in comparison to those fabricated by addition of silica NPs to the PAN solution via ex-situ method for the same silica loadings. For example, the water absorption of FM1 (ex-situ method) is 36.5 % higher than that of FM18 (as seen in Figure 12(a)), while it is 57.4 % higher for FM5 (in-situ method) in comparison to FM18 as illustrated in Figure 12(b). In the similar way for the electrospun films, FM2 (ex-situ method) has increased the absorption of water by 16 %, while the water uptake ratio in FM6 (in-situ method) has been enhanced by 20 % as indicated in Figure 12(c). Better dispersion of silica NPs into the polymeric films and well grafted of the silica NPs into the PAN polymer via chemical bands lead to this higher water absorption.

Effect of Functionalization of NPs

As mentioned earlier, since the surface tension of EG is more than the PAN solutions, the addition of EG to the PAN solutions causes an increase in the surface tension of the polymeric solution and they could not be electrospun. Thus, functionalization of silica NPs is only applied in the casted layers. The water uptake ratio of the films containing EG is given in Figure 12(d). All of the films have the same structure (casted layers) and equal amount of silica loadings. They are compared to FM11, which is also fabricated by casting of the polymer solution and has same amount of silica NPs but it does not contain any EG. It is seen that the films contain EG absorb more water in comparison to the sample without EG. For instance the water absorption in the sample containing 25 wt.% EG/silica NPs (FM13) has been increased by 13 % and this enhancement is more for the NCFs containing higher concentration of EG. EG has two hydroxyl group in its structure and these groups are very strong absorbents for water molecules.

In summary, three factors cause the enhancement of water absorption in the fabricated polymeric films. The first is the electrospinning methodology that makes the polymers to be fabricated in nanoscale size and contribute the higher porosity of electrospun films compared to casted layers. The second factor is the incorporation of silica NPs (via both ex-situ and in-situ methods), which increases the FFV of polymer and leads to an increase in the porosity of polymeric films. Besides, the affinity for absorption of water molecules by fabricated films is also enhanced. The high porous films have much higher surface interactions with water molecules than low porous ones (casted layers) due to the increase in the chemical potential of the system. At the surfaces, van der Waals, electrostatic and hydration interactions result in a positive contribution of chemical potential and lead to manifest itself as an increase in water concentration [74]. The third factor in the enhancement of water absorption is the addition of EG to the samples. Glycols contain hydroxyl groups in their structure that give them a wide variety of derivatives. Hydroxyl group permits EG to act as an intermediate in a wide range of reactions [75,76]. The second advantage of EG is the functionalization of silica NPs. This functionalization increases the solubility of active penetrants (H_2O molecules) in the hybrid matrix and maximizes the compatibility of the two phases in the polymeric films [77].

Water Vapor Transport through Nanocomposite Membranes

The potential of the fabricated NCFs in the absorption of water molecules motivated us to measure the water vapor and methane permeation of the nanocomposite membranes. Figure 13 represents the permeance of water vapor, CH_4 and the selectivity of H_2O/CH_4. The feed flow rate is 3.5 NL min^{-1} at 2.5 bar and 26 °C and the sweep gas flow rate is 3.0 NL min^{-1} at 30 kpa and 24 °C. As mentioned in previous works, the permeance of methane in MEM1 is close to the intrinsic properties of Pebax 1657 polymer [27,78,79], indicating that the fabricated membranes are defect-free. Besides, the actual thickness of NCM selective layers is determined using FESEM and KLONK image software. By measuring the selective layers thickness at 10 different point randomly and taking the average value, the actual thickness of NCM selective layers was 3.12±0.23 μm. In comparison with water vapor permeance of other works, it is found that the equilibrium permeance of water vapor through the membrane without NPs (MEM1) is about four times the permeance of water vapor in membranes that used microporous polymers in their supports layers [27]. This enhancement is believed to be due to utilizing of electrospinning method for fabrication of membrane support layers, which contribute to a high porosity and hence low resistance to water vapor transition through the layers. In another study, Akhtar *et al.* [28] reported 4680 GPU for the permeance of water vapor

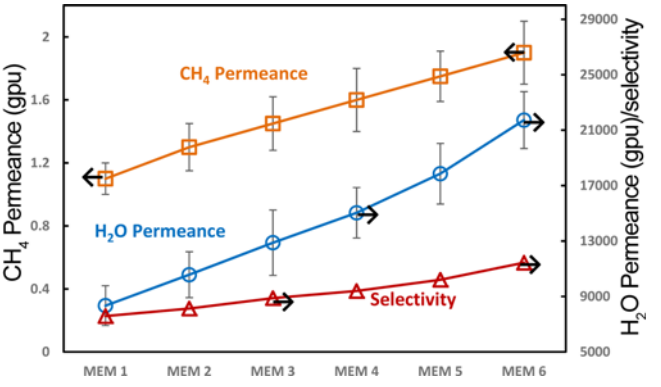

Figure 13. Permeance and selectivity of the fabricated membranes; —○— Water vapor permeance, —□— CH_4 permeance, —Δ— H_2O/CH_4 selectivity.

through pure Pebax 1657 membrane, while the permeance of water vapor for pure Pebax 1657 (MEM1) in present study was 8340 GPU. The difference is related to the higher thickness of their membrane selective layer (5.7 μm).

Incorporation of silica NPs to Pebax 1657 contribute to the increase of both water vapor and methane permeances. In comparison to the membrane without NPs (MEM1), increasing the silica NPs concentration to 30 wt.% (MEM4), enhanced the permeance to about 80 % and 45 % for water vapor and methane gas, respectively. The specific property of the prepared membranes, which can improve the membrane performance and affect the permeability and mass transport of the gases, is the fractional free volume of the selective layers. FFV of the fabricated selective layers was determined based on equations (4) and (5) and are reported in Table 4. The value of V_w=95.09 cm^3/mol is obtained for Pebax 1657, based on Bondi's group contribution method [66,67]. As can be seen, there is an increasing trend for the calculated FFVs by rasing the concentration of non-functionalized silica and functionalized silica NPs. This enhancement in FFVs of the selective layers can give some proofs for improving the properties of NCMs. The increase in methane permeance is due to the increase of membrane fractional free volume and the increase in water vapor permeance is related to both fractional free volume of the membranes and the hydrophilic nature of silica NPs. In previous works, graphene oxide (GO) was incorporated into the membrane selective layers for water vapor permeation tests. A concentration of 2 wt.% of GO nanosheets in Pebax 1657 decreased the water vapor permeance by about 12 % [28] and the water vapor permeance of natural rubber membrane was reduced to 40 % after incorporation of 1.78 vol% graphene as filler [80]. GO is considered as a two dimensional nanoparticle, while CNTs and silica NPs are considered as one dimensional nanoparticles. As a result, the hydrogen bonding in GO is greater than CNTs and silica NPs, making it to aggregate faster in the solvents [81,82].

Functionalization of silica NPs by using EG (MEM5 and 6) also magnified the permeance of water vapor and CH_4 gas. This enhancement in MEM6 was about 45 % for water vapor and 20 % for methane gas with respect to samples without EG (MEM4). Ethylene glycol has two hydroxyl groups in its structure, which are ready to absorb water molecules via hydrogen bonds. The selectivity of fabricated membranes is also increased by the addition of silica NPs and EG to Pebax 1657 copolymer. This increase in the selectivity is due to more permeation of water vapor in comparison to CH_4. The water vapor permeance greater than 10000 GPU corresponds to a performance higher than the currently available commercial materials as mentioned in the work of Huizing *et al.* [83]. By functionalizing the silica NPs with EG and using the sol-gel method for incorporating the NPs into the polymer matrix, the fabricated membranes in this study provide more than twice of H_2O permeance in comparison to commercially available materials.

Conclusion

Appropriate dispersion of nanoparticles can affect industrial processes. The incorporation of silica NPs into PAN and Pebax 1657 films have been studied in this work. The ex-situ incorporation method is not able to properly disperse the NPs even at low loadings. The sol-gel method attenuated the agglomeration process of silica NPs and improved their dispersion at moderate loadings. By using this method, silica NPs grafted well into PAN polymer and enhanced the water absorption and water vapor permeation processes. This enhancement could be applicable for industrial textile and dehydration processes. For higher loadings of NPs, functionalization of NPs is suited well and silica NPs have been functionalized successfully by EG. By using this method, a perfect dispersion of silica NPs was attained at 50 wt.% of NPs. Electrospinning of polymer solutions improved both distributions of NPs into NCFs and the water absorption process due to creating high porosity of NCFs. The NCMs showed a high tendency for water vapor separation from gas mixtures processes, which is comparable to commercially available materials. In this study, we focused on the incorporation of the silica NPs into the polymers to gain good NPs dispersion at moderate and high loadings of NPs. The effect of process parameters on gas dehydration process such as sweep gas flow rate, moisture content in the feed, feed pressure effect and the effect of heavier hydrocarbons such as propane and butane in the feed will be considered in the future work.

Nomenclature

P: Permeability (barrer)
N: Flux (cm^3 s^{-1})
l: Film thickness (cm)
A: Surface area (cm^2)
P_1: Downstream pressure (cmHg)
P_2: Upstream pressure (cmHg)
w: Sample weight (g)
Δw: Water uptake ratio
ρ: Water density (g cm^{-3})
ø: Film porosity
FFV: Fractional free volume
M_{PAN}: Molar weight of a monomer of PAN ($gmo^{-1}l$)
ρ_{PAN}: Density of pure PAN (gcm^{-1})
V_{NCFs}: Specific volume of NCFs (cm^3g^{-1})
φ_{sio2}: Volume fraction of the silica NPs

References

1. V. Srivastava, D. Gusain, and Y. C. Sharma, *Ceram. Int*., **39**, 9803 (2013).

2. T. Y. Chung, M. M. Ba-Abbad, A. W. Mohammad, and A. Benamor, *Desalin. Water Treat.,* **57**, 1 (2016).
3. C. L. Wu, M. Q. Zhang, M. Z. Rong, and K. Friedrich, *Compos. Sci. Technol*., **65**, 635 (2005).
4. J. P. Yang, Z.-K. Chen, G. Yang, S.-Y. Fu, and L. Ye, *Polymer (Guildf)*, **49**, 3168 (2008).
5. Y. Ni, S. Zheng, and K. Nie, *Polymer (Guildf)*, **45**, 5557 (2004).
6. C. L. Chiang, R. C. Chang, and Y. C. Chiu, *Thermochim. Acta*, **453**, 97 (2007).
7. N. Setoodeh, P. Darvishi, and A. Lashanizadegan, *J. Dispers. Sci. Technol*., doi.org/10.1080/01932691.2017.
8. N. Setoodeh, P. Darvishi, and A. Lashanizadegan, *J. Dispers. Sci. Technol*., **39**, 452 (2017).
9. X. J. Shi, G. M. Cai, and W. D. Yu, *Fiber. Polym*., **14**, 1354 (2013).
10. A. A. Voevodin, R. A. Vaia, S. T. Patton, S. Diamanti, M. Pender, M. Yoonessi, J. Brubaker, J. J. Hu, J. H. Sanders, B. S. Phillips, and R. I. MacCuspie, *Small*, **3**, 1957 (2007).
11. D. Kim and L. A. Archer, *Langmuir*, **27**, 3083 (2011).
12. K. Y. A. Lin and A. H. A. Park, *Environ. Sci. Technol*., **45**, 6633 (2011).
13. T. V. Sreekumar, T. Liu, B. G. Min, H. Guo, S. Kumar, R. H. Hauge, and R. E. Smalley, *Adv. Mater*., **16**, 58 (2004).
14. J. J. Ge, H. Hou, Q. Li, M. J. Graham, A. Greiner, D. H. Reneker, F. W. Harris, and S. Z. D. Cheng, *J. Am. Chem. Soc*., **126**, 15754 (2004).
15. Y. Wang, Q. Yang, G. Shan, C. Wang, J. Du, S. Wang, Y. Li, X. Chen, X. Jing, and Y. Wei, *Mater. Lett*., **59**, 3046 (2005).
16. S. Kedem, S. Schmidt, Y. Paz, and Y. Cohen, *Langmuir*, **21**, 5600 (2005).
17. J. Bai, Y. Li, S. Yang, J. Du, S. Wang, C. Zhang, Q. Yang, and X. Chen, *Nanotechnology*, **18**, 305601 (2007).
18. C. A. Bonino, L. W. Ji, Z. Lin, O. Toprakci, X. W. Zhang, and S. A. Khan, *ACS Appl. Mater. Interfaces*, **3**, 2534 (2011).
19. T. Pirzada, S. A. Arvidson, C. D. Saquing, S. S. Shah, and S. A. Khan, *Langmuir*, **30**, 15504 (2014).
20. J. M. Lim, J. H. Moon, G. R. Yi, C. J. Heo, and S. M. Yang, *Langmuir*, **22**, 3445 (2006).
21. L. Ji and X. Zhang, *Mater. Lett*., **62**, 2165 (2008).
22. H. R. Jung, D. H. Ju, W. J. Lee, X. Zhang, and R. Kotek, *Electrochim. Acta*, **54**, 3630 (2009).
23. L. Ji, C. Saquing, S. Khan, and X. Zhang, *Nanotechnology*, **19**, 85605 (2008).
24. D. Rana, B. M. Mandal, and S. N. Bhattacharyya, *Macromolecules*, **29**, 1579 (1996).
25. D. Rana, B. M. Mandal, and S. N. Bhattacharyya, *Polymer (Guildf)*, **37**, 2439 (1996).
26. D. Rana, B. M. Mandal, and S. N. Bhattacharyya, *Polymer (Guildf)*, **34**, 1454 (1993).
27. H. Lin, S. M. Thompson, A. Serbanescu-Martin, J. G. Wijmans, K. D. Amo, K. A. Lokhandwala, and T. C. Merkel, *J. Memb. Sci.,* **413-414**, 70 (2012).
28. F. H. Akhtar, M. Kumar, and K.-V. Peinemann, *J. Memb. Sci*., **525**, 187 (2017).
29. F. K. Ko and Y. Wan, "Introduction to Nanofiber Materials", Cambridge University Press, New York, 2014.
30. S. J. Poormohammadian, P. Darvishi, and A. M. G. Dezfuli, *Chinese J. Chem. Eng.,* In Press (2018).
31. L. P. Esteves, *Cem. Concr. Compos*., **33**, 717 (2011).
32. F. Yalcinkaya, B. Yalcinkaya, A. Pazourek, J. Mullerova, M. Stuchlik, and J. Maryska, *Int. J. Polym. Sci*. doi:10.1155/2016/4671658.
33. S. Metz, W. Vandeven, J. Potreck, M. Mulder, and M. Wessling, *J. Memb. Sci*., **251**, 29 (2005).
34. S. J. Metz, W. J. C. Van De Ven, M. H. Mulder, and M. Wessling, *J. Memb. Sci*., **266**, 51 (2005).
35. H. Sijbesma, K. Nymeijer, R. Van Marwijk, R. Heijboer, J. Potreck, and M. Wessling, *J. Memb. Sci*., **313**, 263 (2008).
36. V. I. Bondar, B. D. Freeman, and I. Pinnau, *J. Polym. Sci. Part B Polym. Phys*., **37**, 2463 (1999).
37. P. S. Goh, A. F. Ismail, and B. C. Ng, *Desalination*, **308**, 2 (2013).
38. L. Ansaloni and L. Deng, *Recent Dev. Polym. Macro, Micro Nano Blends Prep. Characterisation*, **163** (2016).
39. M. Jacoby, *Chem. Eng. News*., **91**, 34 (2013).
40. S. K. Henninger, F. Jeremias, H. Kummer, P. Schossig, and H.-M. Henning, *Energy Procedia*, doi:10.1016/j.egypro. 2012.11.033.
41. C. R. Wade, T. Corrales-Sanchez, T. C. Narayan, and M. Dincă, *Energy Environ*. *Sci*., **6**, 2172 (2013).
42. H. C. Zhou, J. R. Long, and O. M. Yaghi, *Chem. Rev*., **112**, 673 (2012).
43. A. I. Skoulidas, D. M. Ackerman, J. K. Johnson, and D. S. Sholl, *Phys. Rev. Lett*., **89**, doi:10.1103/PhysRevLett.89. 185901.
44. M. Cinke, J. Li, C. W. Bauschlicher, A. Ricca, and M. Meyyappan, *Chem. Phys. Lett*., **376**, 761 (2003).
45. A. H. El-Sheikh, J. A. Sweileh, Y. S. Al-Degs, A. A. Insisi, and N. Al-Rabady, *Talanta*, **74**, 1675 (2008).
46. T. A. Kotel'nikova, *Russ. J. Phys. Chem. A*., **91**, 1301 (2017).
47. M.-J. Wang, S. Wolff, and J.-B. Donnet, *Rubber Chem. Technol*., **64**, 714 (1991).
48. C. Brinker and G. Scherer, "Sol-Gel Science: The Physics and Chemistry of Sol-Gel Processing", Academic Press, San Diego, 1990.
49. K. M. Sawicka and P. Gouma, *J. Nanoparticle Res*., **8**, 769 (2006).
50. J. Gao, T. Gao, and M. J. Sailor, *Appl. Phys. Lett*., **77**, 901 (2000).
51. H. Nagel and R. Hezel, *Sol*. *Energy Mater. Sol. Cells*., **65**, 71 (2001).
52. P. Rittigstein, R. D. Priestley, L. J. Broadbelt, and J. M. Torkelson, *Nat. Mater*., **6**, 278 (2007).
53. T. Kang, J. H. Lee, and S. G. G. Oh, *J. Ind. Eng. Chem*., **46**,

289 (2017).
54. N. A. M. Barakat, M. F. Abadir, F. A. Sheikh, M. A. Kanjwal, S. J. Park, and H. Y. Kim, *Chem. Eng. J.,* **156**, 487 (2010).
55. Y. Du, S. Z. Shen, K. Cai, and P. S. Casey, *Prog. Polym. Sci.,* **37**, 820 (2012).
56. C. L. Lu and B. Yang, *J. Mater. Chem*., **19**, 2884 (2009).
57. R. Ciriminna, A. Fidalgo, V. Pandarus, F. B. land, L. M. Ilharco, M. Pagliaro, F. Béland, L. M. Ilharco, and M. Pagliaro, *Chem. Rev*., **113**, 6592 (2013).
58. S. Kango, S. Kalia, A. Celli, J. Njuguna, Y. Habibi, and R. Kumar, *Prog. Polym. Sci*., **38**, 1232 (2013).
59. M. Iijima, M. Kobayakawa, M. Yamazaki, Y. Ohta, and H. Kamiya, *J. Am. Chem. Soc*., **131**, 16342 (2009).
60. T. Yadav, A. A. Mungray, and A. K. Mungray, *RSC Adv*., **5**, 64421 (2015).
61. A. K. Mungray and P. Kumar, *J. Environ. Manage*., **88**, 995 (2008).
62. W. Stöber, A. Fink, and E. Bohn, *J. Colloid Interface Sci*., **26**, 62 (1968).
63. S. Kiatkamjornwong, W. Chomsaksakul, and M. Sonsuk, *Radiat. Phys. Chem*., **59**, 413 (2000).
64. B. P. Tripathi, N. C. Dubey, R. Subair, S. Choudhury, and M. Stamm, *RSC Adv*., **6**, 4448 (2016).
65. Y. Shen and A. C. Lua, *Chem. Eng. J.,* **188**, 199 (2012).
66. A. Bondi, *J. Phys. Chem*., **68**, 441 (1964).
67. Y. H. Zhao, M. H. Abraham, and A. M. Zissimos, *J. Org. Chem*., **68**, 7368 (2003).
68. A. Jomekian, R. M. Behbahani, T. Mohammadi, and A. Kargari, *Korean J. Chem. Eng*., **34**, 440 (2017).
69. S. W. Choi, J. R. Kim, S. M. Jo, W. S. Lee, and Y. R. Kim, *J. Electrochem. Soc*., **152**, A989 (2005).
70. B. D. Cullity and S. R. Stock, "Elements of X-ray Diffraction", Massachusets, Addison-Weswly Publishing Company, 2001.
71. S. C. George and S. Thomas, *Prog. Polym. Sci*., **26**, 985 (2001).
72. D. F. Shao, Q. F. Wei, L. W. Zhang, Y. B. Cai, and S. D. Jiang, *Appl. Surf. Sci.,* **254**, 6543 (2008).
73. J. Gao, X. Wang, J. Zhang, and R. Guo, *Sep. Purif. Technol*., **159**, 116 (2016).
74. B. D. Vogt, C. L. Soles, R. L. Jones, C. Y. Wang, E. K. Lin, W. Wu, S. K. Satija, D. L. Goldfarb, and M. Angelopoulos, *Langmuir*, **20**, 5285 (2004).
75. Y. Yang, D. Rana, C. Q. Lan, and T. Matsuura, *ACS Appl. Mater. Interfaces*., **8**, 15778 (2016).
76. Y. Yang, D. Rana, and C. Q. Lan, *RSC Adv*., **5**, 59583 (2015).
77. S. Janakiram, M. Ahmadi, Z. Dai, L. Ansaloni, and L. Deng, *Membranes (Basel)*, doi:10.3390/membranes8020024.
78. P. I. Blume, *US Patent*, US4963165 A (1990).
79. I. Pinnau and L. G. Toy, *J. Memb. Sci.,* **184**, 39 (2001).
80. Y. Zhan, M. Lavorgna, G. Buonocore, and H. Xia, *J. Mater. Chem*., **22**, 10464 (2012).
81. A. Ammar, A. M. Al-Enizi, M. A. AlMaadeed, and A. Karim, *Arab. J. Chem*., **9**, 274 (2016).
82. D. H. Kim, Y. S. Yun, and H. J. Jin, *Curr. Appl. Phys*., **12**, 637 (2012).
83. R. Huizing, W. Mérida, and F. Ko, *J. Memb. Sci*., **461**, 146 (2014).